1 Formalism of non-standard interactions

Non-standard interactions are sub-leading contributions to neutrino flavor transitions arising from neutrino interactions not considered in the Standard Model. We consider matter NSIs arising from the neutral current NSIs, which exclude production and detection effects. An effective four-fermion Lagrangian for this type of interaction can be written as

$$\mathcal{L}_{\rm NC} = -2\sqrt{2}G_F\epsilon^{fX}_{\alpha\beta}\left(\bar{\nu}_\alpha\gamma^\mu P_L\nu_\beta\right)\left(\bar{f}\gamma_\mu P_X f\right)\,, \tag{1}$$

where NC denotes the neutral current interaction with $f \in \{e, u, d\}$, and P_X is the chirality projection operators with $X \in \{L, R\}$.

For chirality X, the NSI Hamiltonian takes the form

$$H = \frac{1}{2E}UM^2U^\dagger + \sqrt{2}G_F n_e \mathrm{diag}(1,0,0) + \sqrt{2}G_F\sum_f n_f\epsilon^{fX} \tag{2}$$

We have no independent sensitivity for the chirality of ϵ^{fX}, so we sum over these to obtain the vectorial parameter as $\epsilon^{fV}_{\alpha\beta} = \epsilon^{fL}_{\alpha\beta} + \epsilon^{fR}_{\alpha\beta}$. Moreover, we normalize the fermion number density n_f by the electron number density n_e. Our matter study will be wholly confined to the interior of the Earth, where we assume electrical neutrality and equal distribution of neutrons and protons, so we use the relations $n_u/n_e \simeq n_d/n_e \simeq 3$. The effective NSI parameters in matter now take the form

$$\begin{aligned}\epsilon_{\alpha\beta} &= \sum_{X\in\{L,R\}}\sum_{f\in\{e,u,d\}}\frac{N_f}{N_e}\epsilon^{fX}_{\alpha\beta} \\ &= \sum_X \epsilon^{eX}_{\alpha\beta} + 3(\epsilon^{uX}_{\alpha\beta} + \epsilon^{dX}_{\alpha\beta})\end{aligned} \tag{3}$$

We note that our definition of $\epsilon_{\alpha\beta}$ differs from e.g. [1], where the quark number density is used to normalize the parameters.

With the matter potential $V = \sqrt{2}G_F n_e$, we write

$$H = \frac{1}{2E}UM^2U^\dagger + V\begin{bmatrix}1+\epsilon_{ee} & \epsilon_{e\mu} & \epsilon_{e\tau}\\ \epsilon_{e\mu} & \epsilon_{\mu\mu} & \epsilon_{\mu\tau}\\ \epsilon_{e\tau} & \epsilon_{\mu\tau} & \epsilon_{\tau\tau}\end{bmatrix}\,, \tag{4}$$

where we have assumed the components of the NSI matrix to be real.

To propagate the neutrino states through the Earth, we solve the Schrödinger equation with the Hamiltonian from Eq. 4. The Earth density profile is taken from the PREM [2], and we do not consider neutrino absorption. The baseline for a given trajectory is determined using an average neutrino production height of 15 km and an Earth radius of 6371 km. Thus, matter oscillations introduce a zenith angle dependence in two areas. Firstly, the matter potential depends on the matter density through the neutrino propagates. A neutrino with $\cos\theta_z < -0.87$ will traverse through the dense Earth core, whereas a mantle-crossing neutrino with $\cos\theta_z > -0.87$ will not. Secondly, the zenith angle also alters the baseline through which a neutrino undergoes matter oscillations. After this, we are ready to study the NSI effect on probability level.

1.1 NSI phenomenology at probability level

The atmospheric $\nu_\mu \to \nu_\tau$ transition will be the most abundant, making $\epsilon_{\mu\tau}$, $\epsilon_{\mu\mu}$, $\epsilon_{\tau\tau}$ the most suitable NSI parameters to constrain from muon events. As we will see, $\epsilon_{e\mu}$ is also a good candidate to constrain, albeit a weaker one.

In Fig. 1, we see how the introduction of $\epsilon_{\mu\tau} = 0.02$ alters the ν_μ and $\bar{\nu}_\mu$ survival probabilities for neutrinos that traverse the entire Earth diameter (i.e. $\cos(\theta_z^T) = -1$). $\epsilon_{\mu\tau}$ does not dramatically change neither amplitude nor frequency of the probabilities. Instead, it seems to stretch or compress the oscillations. Since the only difference between the way neutrinos and antineutrinos interact with matter is the sign of the potential, the probability for ν_μ with positive $\epsilon_{\alpha\beta}$ is identical to the probability for $\bar{\nu}_\mu$ with negative $\epsilon_{\alpha\beta}$. Thus, the dashed line in the right panel not only shows the survival probability for $\bar{\nu}_\mu$ with $\epsilon_{\mu\tau} = 0.02$, but also the survival probability for ν_μ with $\epsilon_{\mu\tau} = -0.02$. Hence, we note that $\epsilon_{\mu\tau} > 0$ stretches (compresses) $P_{\mu\mu}$ for neutrinos (antineutrinos), while $\epsilon_{\mu\tau} < 0$ compresses (stretches) $P_{\mu\mu}$ for neutrinos (antineutrinos).

The value of $\epsilon_{\tau\tau}$ affects neither $P_{\mu\mu}$ nor $P_{\bar{\mu}\bar{\mu}}$, in the IceCube region above 500 GeV. Hence, we will not be able to say anything about $\epsilon_{\tau\tau}$ in our IceCube study. Comparing the probabilities in Fig. 1 with $\epsilon_{\tau\tau} = 0.05$ with the ones for $\epsilon_{\mu\tau} = 0.02$ in Fig. 1, we see that even though we let $\epsilon_{\tau\tau}$ take 2.5 times the value of $\epsilon_{\mu\tau}$, its effect on $P_{\mu\mu}$ is smaller. The weakening of the $P_{\bar{\mu}\bar{\mu}}$ resonance will be visible in DeepCore, but we should expect a less stringent constraint due to the weakness of the effect compared to $\epsilon_{\mu\tau}$.

Thus, we will use IceCube to constrain $\epsilon_{\mu\tau}$ only.

Moving on to $\epsilon_{e\mu}$ and Fig. 2, we see that both probabilities has shifted downwards for $E^T > 500$ GeV. In Fig. 2, we see that the muon channel remains largely unaffected of the value of $\epsilon_{e\tau}$ as we expected. The exception of this lies in the DeepCore region of rapid oscillations, where mixing is more violent.

The effect of NSI on the DeepCore event count has been previously discussed in [3], while the NSI effect in PINGU has been studied in [4, 5]. Now we repeat our probability analysis but for the DeepCore/PINGU region of 5.6 GeV to 56 GeV. As we previously saw, we have rapid oscillations, which means that 'indirect' modifications (i.e. $\epsilon_{e\tau}$ will affect the $P_{\mu\mu}$ channel) will be more apparent since all flavors are involved to a greater degree compared with the more stable region above 500 GeV, where many oscillations have averaged out.

Another feature of our DeepCore study includes the fact that we now have access to cascade events, in which ν_e and ν_τ are more abundant. Thus, we are no longer constrained to the μ channel alone, but we can now find interesting features in the other channels too. However, we remember that the ν_μ flux is still the most abundant.

Fig. 4 shows the electron neutrino and antineutrino survival probabilities, and here we see a clear signal when turning on $\epsilon_{e\tau}$.

Fig. 1 shows that $\epsilon_{\mu\tau}$ affects both $P_{\mu\mu}$ and $P_{\bar{\mu}\bar{\mu}}$ over the whole energy range. Since IceCube also sees this, we hope to be able to boost the constraining of $\epsilon_{\mu\tau}$ by combining the two experiments.

Regarding $\epsilon_{\tau\tau}$ in Fig. 2, the signal mainly shows in the $P_{\bar{\mu}\bar{\mu}}$ channel as a

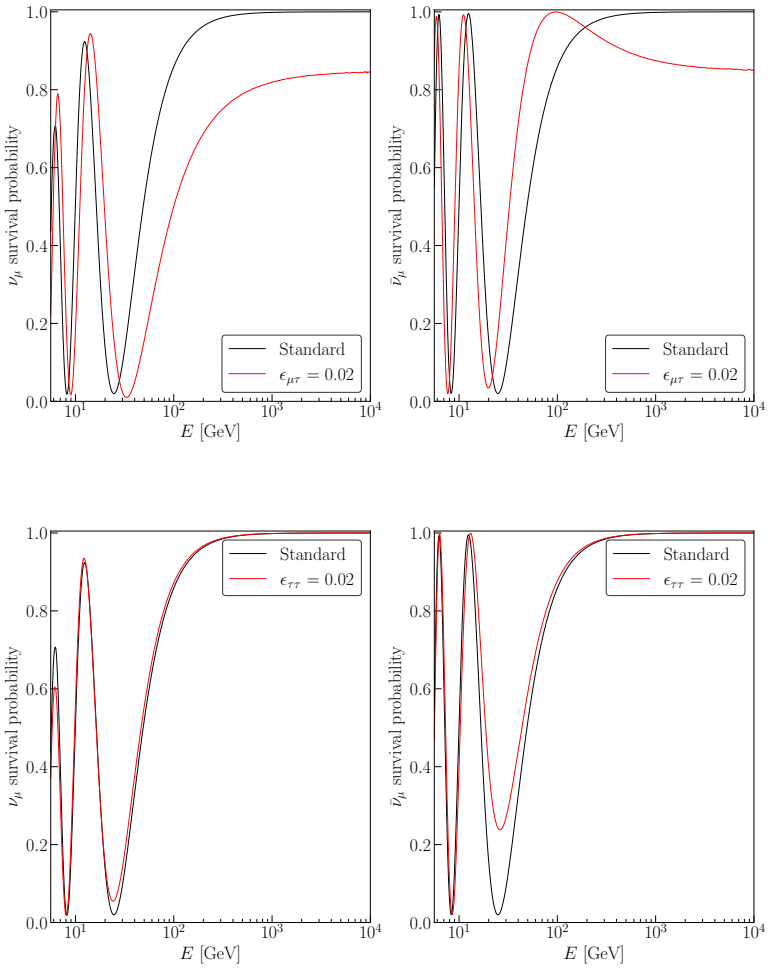

Figure 1: *Top panel:* Muon neutrino and antineutrino survival probabilities for $\cos(\theta_z^T) = -1$ when $\epsilon_{\mu\tau} = 0.02$. All other NSI parameters are fixed to zero. In the GeV range, $\epsilon_{\mu\tau}$ shifts the oscillations to the right for ν_μ, and to the left for $\bar{\nu}_\mu$. At TeV energies, both probabilities simply get shifted down, resulting in a net reduction of track events. *Bottom panel:* Muon neutrino and antineutrino survival probabilities for $\cos(\theta_z^T) = -1$ when $\epsilon_{\tau\tau} = 0.05$. All other NSI parameters are fixed to zero. $\epsilon_{\tau\tau}$ does not affect the probabilities above 100 GeV and this parameter is thus unable to be constrained by tracks in IceCube in our study. However, the dampening of the $\bar{\nu}_\mu$ survival probability will be visible to DeepCore and PINGU, since it occurs within their energy ranges.

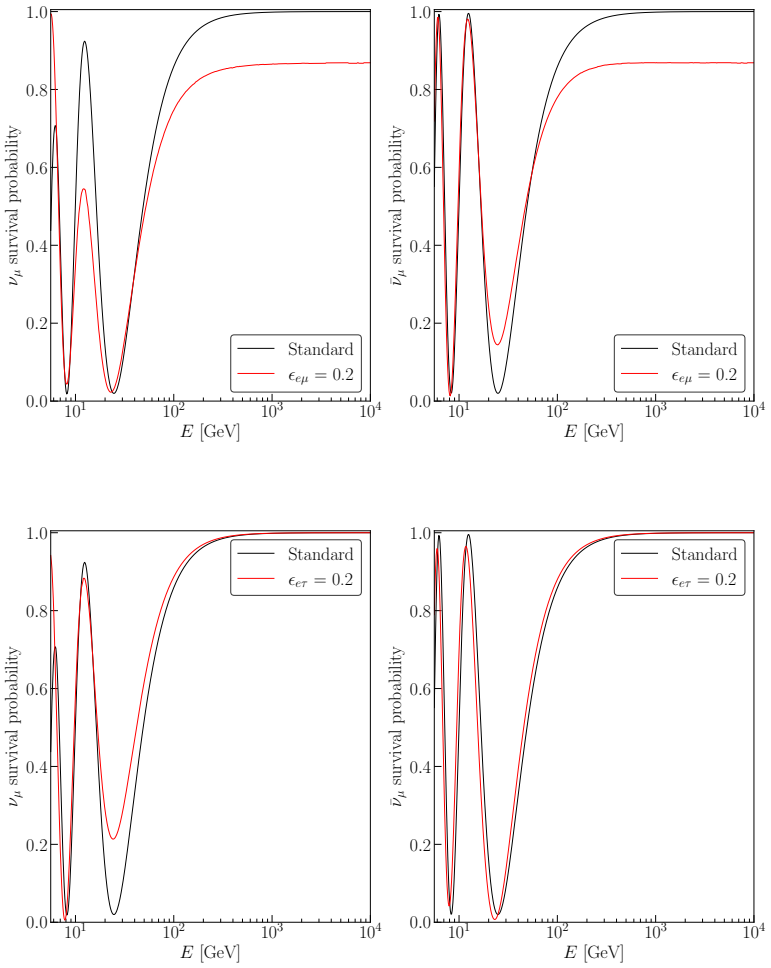

Figure 2: Muon neutrino and antineutrino survival probabilities for $\cos(\theta_z^T) = -1$. *Top panel:* $\epsilon_{e\mu} = 0.2$. All other NSI parameters are fixed to zero. Instead of the oscillations shifting to the left or right, $\epsilon_{e\mu}$ dampens an oscillation peak for low GeV. At TeV, the probability is shifted down, just as with $\epsilon_{\mu\tau}$. *Bottom panel:* $\epsilon_{e\tau} = 0.2$. All other NSI parameters are fixed to zero. Here, we see a very weak shifting and a ν_μ weaker dip at low GeV, and again, no visible effect at TeV energies.

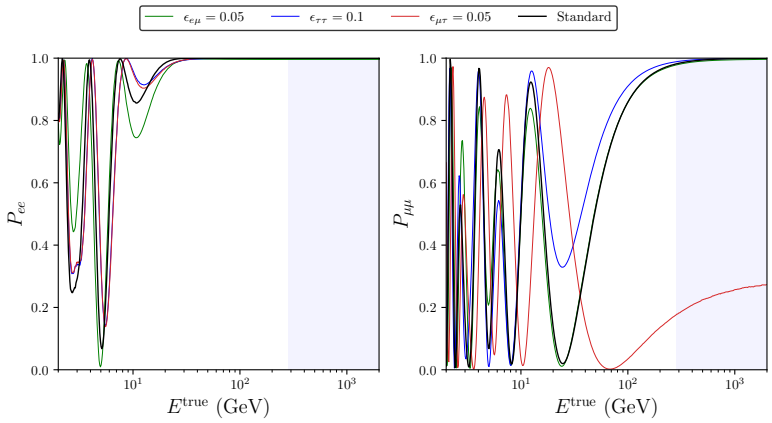

Figure 3

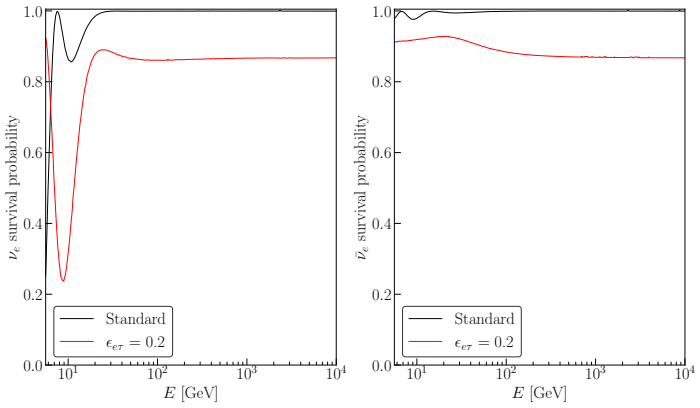

Figure 4: Electron neutrino and antineutrino survival probabilities for $\cos(\theta_z^T) = -1$ when $\epsilon_{e\tau} = 0.2$. All other NSI parameters are fixed to zero. Here we see a strong difference across the whole energy range, in contrast to the ν_μ and $\bar{\nu}_\mu$ plots in Fig 2.

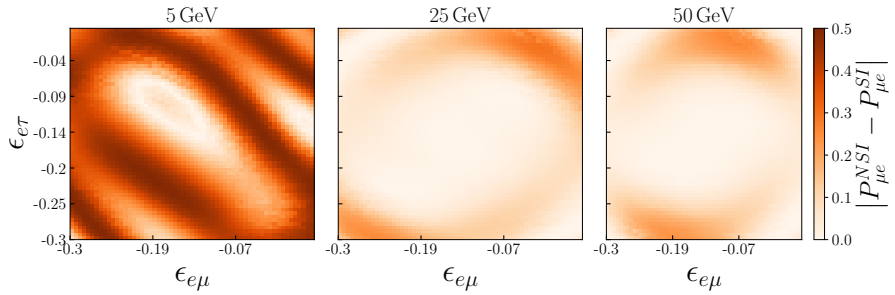

Figure 5: The quantity $\left|P_{\mu e}^{NSI} - P_{\mu e}^{SI}\right|$ when we let $\epsilon_{e\mu}$ and $\epsilon_{e\tau}$ independently vary over the range {-0.3,0.3} at 5, 25, and 50 GeV. At 5 GeV, we see strong deviations in the probabilities, showing a promising indication that constriction of $\epsilon_{e\mu}$ and $\epsilon_{e\tau}$ is possible using cascade events at these energies.

shallower dip in the 20 GeV region. Thus, DeepCore/PINGU alone will be used to constrain this parameter.

$\epsilon_{e\mu}$ in Fig. 2 causes a weaker dip for both ν_μ and $\bar{\nu}_\mu$.

For $\epsilon_{e\tau}$, we see a similar effect on the dip in $P_{\mu\mu}$ as we did with $\epsilon_{\tau\tau}$ for $P_{\bar{\mu}\bar{\mu}}$. Hence, we should be able to see the $\epsilon_{e\tau}$ effect in DeepCore/PINGU. Remember that we now have the option to look at the other flavor channels than μ since we have cascade events for DeepCore and PINGU. If we simulate $P_{\mu e}^{NSI}$ at three different energies, and let both $\epsilon_{e\mu}$ and $\epsilon_{e\tau}$ vary together between the values $\{-0.3, 0.3\}$, we produce a two-dimensional grid of probabilities. Subtract the regular $P_{\mu e}^{SI}$ (that is, no NSI), and take the absolute value of the difference. We see the result in Fig. 5. The middle and right panels, which show the absolute probability difference at 25 and 50 GeV, respectively, are very bleak, indicating that the impact of the NSI parameters $\epsilon_{e\mu}$ and $\epsilon_{e\tau}$ is not as strong at these energy levels. Turning to the left-most panel, we see a region in which the difference again is close to zero, but now surrounded by fringes of very large differences, up to 50% difference in the $P_{\mu e}$ probability. This indicates that the NSI parameters are much more influential at these energies, and that we should be able to constrain both $\epsilon_{e\mu}$ and $\epsilon_{e\tau}$ from 5 GeV cascade events.

1.2 NSI phenomenology at flux level

To study the NSI flux effect, we propagate the atmospheric neutrino flux from Honda et al [6] through the Earth. The oscillation probability $P_{\alpha\beta}$ acts as a weight to the atmospheric flux, yielding the propagated flux for flavor β at detector level as

$$\phi_\beta^{\text{det}} = \sum_\alpha P_{\alpha\beta}\phi_\alpha^{\text{atm}}\,, \tag{5}$$

where we sum over the initial lepton flavors $\alpha \in \{e, \mu, \bar{e}, \bar{\mu}\}$. To illustrate the impact of $\epsilon_{\mu\tau}$ at flux level, we plot in Fig. 6 the quantity $(\phi_{\nu_\mu}^{NSI} + \phi_{\bar{\nu}_\mu}^{NSI})/(\phi_{\nu_\mu}^{SI} +$

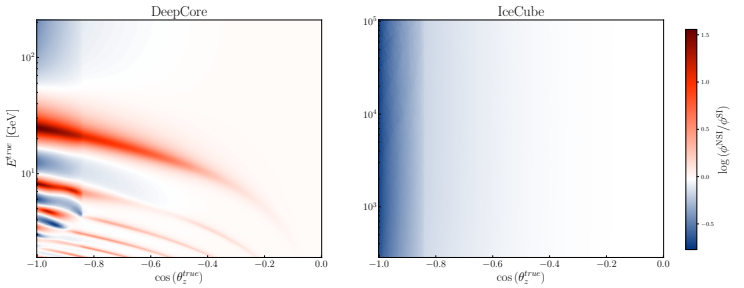

Figure 6: Ratio of detector NSI to SI atmospheric $\nu_\mu + \bar{\nu}_\mu$ fluxes expressed as $(\phi^{NSI}_{\nu_\mu} + \phi^{NSI}_{\bar{\nu}_\mu})/(\phi^{SI}_{\nu_\mu} + \phi^{SI}_{\bar{\nu}_\mu})$. We set $\epsilon_{\mu\tau} = -0.05$, and all other $\epsilon_{\alpha\beta} = 0$. Left (right) panel shows the flux ratio in the energy range in which 99% of the simulated DeepCore (IceCube) events are contained.

$\phi^{SI}_{\bar{\nu}_\mu}$), where all fluxes are propagated to detector level by Eq. 5. In the left (right) panel, we plot the flux in region in which 99% of the DeepCore (IceCube) track events originating from $\nu_\mu + \bar{\nu}_\mu$ fluxes are contained. We see that the only clear signal discernible to the IceCube detector is a energy-independent flux deficiency with a factor in the order of $\sim 10^{0.5}$ from core-crossing neutrinos within a zenith range of $\cos(\theta_z^T) < -0.87$. DeepCore on the other hand, is exposed to multiple fringes of flux surpluses with a factor in the order of ~ 10. The strongest surplus at 20 GeV is very weakly zenith dependent, a stark contrast to the energy-independent but zenith-sensitive IceCube deficiency.

The muonic flux not only carries the largest $\epsilon_{\mu\tau}$ effect, but it is also more abundant than the ν_e flux. Thus, we expect to receive the highest statistics from μ-related NSI parameters, thus constraining them the strongest. $\epsilon_{\alpha\beta}$ which are only indirectly weakly dependent on the μ channel will have the weakest bounds. This could be improved by considering cascade events in IceCube, thus opening up the e and τ channels there.

2 Detector formalism

The IceCube Neutrino Observatory is a gigaton Cherenkov detector located within Antarctic ice near the Geographic South Pole. It consists of 5160 individual digital optical modules situated on 86 strings, which detect Cherenkov light emitted by charged leptons from neutrino events. We distinguish between two interaction topologies: track- and cascade-like events. Track-like events originate mainly from muons originating from ν_μ CC interactions, while cascades predominantly consist of electromagnetic and hadronic showers.

DeepCore is a dense sub-array within the standard IceCube array, which allows us to observe neutrino interactions down to a few GeV [7]. Due to its lower energy threshold compared with IceCube, DeepCore has previously been used to study NSI effects in this more discernible range[7, 1].

PINGU is a proposed 26 string in-fill array to IceCube, consisting of optical modules of similar nature [8]. While proposed to mainly shed light on neutrino mass ordering, PINGU will be able to probe NSI parameters as well.

2.1 IceCube

We obtain the data from the IC-86 sterile data release [9], which contains muon track events collected over 8 years. In the data, the reconstructed energy E^R is logarithmically binned between 500 GeV to 9976 GeV, totalling 13 bins (index i). The reconstructed cosine-zenith $\cos(\theta_z^R)$ is linearly binned between -1 and 0 in 20 bins (index j).

The event count for each bin reads

$$N_{ij} = T \sum_{\beta} \int_{(\cos\theta_z^r)_i}^{(\cos\theta_z^r)_{i+1}} \mathrm{d}\cos\theta_z^r \int_{E_j^r}^{E_{j+1}^r} \mathrm{d}E^r \int_0^{\pi} R(\theta^r, \theta^t) \mathrm{d}\cos\theta^t \int_0^{\infty} R(E^r, E^t) \phi_\beta^{\mathrm{det}} A_\beta^{\mathrm{eff}} \mathrm{d}E^t \,, \tag{6}$$

where T is the live time of the detector, β the final neutrino flavors, θ_z^r the reconstructed zenith angle, i.e. the deduced direction of the incoming neutrino binned with index i. θ_z^t is the true zenith angle of the incoming neutrino. E^r is the reconstructed energy, binned with index j. $R(\theta^r, \theta^t)$ is a zenith resolution function that describes the relationship with the reconstructed and true zenith angles, specific to the 86-string configuration of IceCube. $R(E^r, E^t)$ is an energy resolution function that describes the relationship with the reconstructed and true energies. $\phi_\beta^{\mathrm{det}}$ is the conventional atmospheric neutrino flux for flavor β, propagated to detector level in accordance with Eq. 5. The effective area A^{eff} is binned and provided to us by the IceCube collaboration [10].

For the energy and zenith resolution functions, we assume a log-normal distribution, giving it the form

$$R(x^r, x^t) = \frac{1}{\sqrt{2\pi}\sigma_{x^r} x^r} \exp\left[-\frac{(\log x^r - \mu(x^t))^2}{2\sigma_{x^r}^2} \right] . \tag{7}$$

However, the energy reconstruction is biased, meaning that the most probable reconstructed energy for a given true energy is not the same due to systematic differences [11]. Thus, we don't assume that $\mu(E^T) = E^R$. To model this relationship between E^T and E^R, we fit a Gaussian process regressor on the IC-86 Monte Carlo dataset from [12], from which we can extract a predicted mean and standard deviation for a given E^R. We then take the E^T points of the 99th percentile of each reconstructed distribution to obtain the E^T limits over which to integrate. We take the angular resolution function to be identically unity since the angle resolution in IceCube for track-like events is less than 2°, making $\cos(\theta_z^T)$ practically coincide with $\cos(\theta_z^R)$ for our study [9].

2.2 DeepCore

We use the publically available DeepCore data sample [13] which is an updated version of what was used by the IceCube collaboration in a ν_μ disappearance

analysis [14].

The detector systematics include ice absorption and scattering, as well as overall, lateral, and head-on optical efficiencies of the DOMs. They are applied as correction factors using the best-fit points from the DeepCore 2019 ν_τ appearance analysis [15].

The data include 14901 track-like events and 26001 cascade-like events, both divided into eight $\log_{10} E^R \in [0.75, 1.75]$ bins (index i), eight $\cos(\theta_z^R) \in [-1, 1]$ bins (index j), and two bins for the event classification (index k). Each event has a Monte Carlo weight $w_{ijk,\beta}$ from which we can construct the event count as

$$N_{ijk} = C_{ijk} \sum_\beta w_{ijk,\beta}\, \phi_\beta^{\text{det}}\,, \tag{8}$$

where C_{ijk} is the correction factor from the detector systematic uncertainty and ϕ_β^{det} is defined as Eq. 5. We have now substituted the effect of the Gaussian smearing by treating the reconstructed and true quantities as a migration matrix.

2.3 PINGU

The methodology behind the PINGU simulations is the same as with our DeepCore study 2.2. We use the public Monte Carlo [16], which allows us to construct the event count as in Eq. 8. However, since no detector systematics is yet modeled for PINGU,the correction factors C_{ijk} are all unity. We will remedy this by including an uncorrelated systematic error, which we can scale at will. As with the DeepCore Monte Carlo, the PINGU Monte Carlo is divided into eight $\log_{10} E^R \in [0.75, 1.75]$ bins, and eight $\cos(\theta_z^R) \in [-1, 1]$ bins for both track- and cascade-like events. We plot the normalized event differences $(N_{NSI} - N_{SI})/\sqrt{N_{SI}}$ for cascades and tracks in Fig. 10. We generate 'data' by predicting the event rates at PINGU with the following best-fit parameters from [17], except for the CP-violating phase which is set to zero for simplicity.

$$\begin{aligned} &\Delta m^2_{21} = 7.42 \times 10^{-5}\,\text{eV}^2,\ \ \Delta m^2_{31} = 2.517 \times 10^{-3}\,\text{eV}^2, \\ &\theta_{12} = 33.44^\circ, \quad \theta_{13} = 8.57^\circ, \quad \theta_{23} = 49.2^\circ, \quad \delta_{\text{CP}} = 0\,. \end{aligned} \tag{9}$$

3 Results

At the reconstructed event level, we note that the $\epsilon_{\mu\tau}$ features discussed in Sec. 1.2 display themselves differently in each detector. We investigate this for $\epsilon_{\mu\tau}$ by in Fig. 7a plotting the muon survival probability difference $P_{\mu\mu}(\epsilon^+_{\mu\tau}) - P_{\mu\mu}(\epsilon^-_{\mu\tau})$, where $\epsilon^\pm_{\mu\tau} = \pm 0.01$. Comparing Fig. 7a with the flux ratios in Fig. 7b, we see that the reconstruction of PINGU is superior to DeepCore, since the event ratio $\log(N^+_{NSI}/N^-_{NSI}) = \log N^+_{NSI} - \log N^-_{NSI}$ (in reconstructed quantities) more closely matches the probability difference $P^+ - P^-$ (in true quantities).

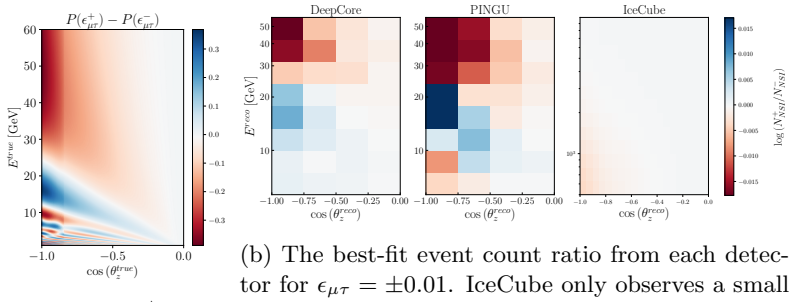

(a) $P_{\mu\mu}(\epsilon^+_{\mu\tau}) - P_{\mu\mu}(\epsilon^-_{\mu\tau})$ using $\epsilon^{\pm}_{\mu\tau} = \pm 0.01$

(b) The best-fit event count ratio from each detector for $\epsilon_{\mu\tau} = \pm 0.01$. IceCube only observes a small surplus of events for $\epsilon_{\mu\tau} = -0.01$ compared to DeepCore and PINGU due to the weak NSI effect at high GeV energies.

Figure 7: Probability difference and best-fit event count. Negative $\epsilon_{\mu\tau}$ has the strongest signal, as the thin blue region stemming from $\epsilon_{\mu\tau} = 0.01$ is less prominent than the red regions from $\epsilon_{\mu\tau} = -0.01$.

This is most evident below 20 GeV, where the DeepCore reconstruction has washed out the fringes while PINGU preserves the N^-_{NSI} surplus below 10 GeV.

Now we turn to the effect of $\epsilon_{\mu\tau}$. Muon events are the most abundant, and it suffices to study $P_{\mu\mu}$ in this way to explain the $\epsilon_{\mu\tau}$ features. First, let $P^{\pm}$ denote $P_{\mu\mu}(\epsilon^{\pm}_{\mu\tau})$. We see see that $\epsilon^+_{\mu\tau}$ generates a slightly higher $P_{\mu\mu}$ for energies around 20 GeV (blue area), while $\epsilon^-_{\mu\tau}$ produces higher $P_{\mu\mu}$ for almost all other combinations of $E^T, \cos(\theta^T_z)$. As we see in Fig. 6, this muon survival abundance is indeed preserved at flux level. So the flux for $\epsilon^+_{\mu\tau}$ is higher than the flux for $\epsilon^-_{\mu\tau}$. Is this still true at event level, i.e. after reconstruction? As we see in Fig. 7b, the binned PINGU event counts display strong differences for many bins, which will give a high statistics on both sides of $\epsilon_{\mu\tau} = 0$, slightly favoring $\epsilon^-_{\mu\tau}$. DeepCore on the other hand has fewer bins where the event count for $\epsilon^-_{\mu\tau}$ surpasses the event count for $\epsilon^+_{\mu\tau}$, giving weaker statistics for the negative side. Thus, we conclude that we will see a $\epsilon_{\mu\tau}$ GeV-asymmetry stemming from the lower statistics for negative $\epsilon_{\mu\tau}$ at probability level, which is then propagated through the flux and finally affects the reconstruction.

3.1 Constraining the NSI parameters

In this section, we will constrain the four NSI parameters $\epsilon_{\tau\tau}$, $\epsilon_{\mu\tau}$, $\epsilon_{e\mu}$, and $\epsilon_{e\tau}$ by considering the detectors separately as well as jointly. For our analyses, we define our χ^2 as

$$\chi^2(\hat{\theta}, \alpha, \beta, \kappa) = \sum_{ijk} \frac{\left(N^{\text{th}} - N^{\text{data}}\right)^2_{ijk}}{\left(\sigma^{\text{data}}_{ijk}\right)^2 + \left(\sigma^{\text{syst}}_{ijk}\right)^2} + \frac{(1-\alpha)^2}{\sigma^2_\alpha} + \frac{\beta^2}{\sigma^2_\beta} \tag{10}$$

where we minimize over the model parameters $\hat{\theta} \in \{\Delta m^2_{31}, \theta_{23}, \epsilon\}$, the penalty terms α and β, and the free parameter κ. N^{th}_{ijk} is the expected number of events

from theory in bin $\{i, j, k\}$, where i denotes the E^R bin, j denotes the $\cos(\theta_z^R)$ bin, and k denotes the event-type bin, i.e. track or cascade. $N_{ijk}^{\rm data}$ is the observed number of events in that bin. $\sigma_{ijk}^{\rm data}$ is the experimental uncertainty, and $\sigma_{ijk}^{\rm syst}$ the uncorrelated systematic uncertainty.

In our simulations of $N_{ijk}^{\rm th}$, we set all standard oscillation parameters to their current best-fit values of Eq. 9, except for Δm_{31}^2[31] and θ_{23} which we vary over their 3σ limits $2.435 \times 10^{-3}\,{\rm eV}^2$ to $2.598 \times 10^{-3}\,{\rm eV}^2$ and 40.1° to 51.7°, respectively [17].

We set $\sigma_\alpha = 0.25$ as the atmospheric flux normalization error, and $\sigma_\beta = 0.05$ as the zenith angle slope error [6]. The observed event number has an associated Poissonian uncertainty $\sigma_{ijk}^{\rm data} = \sqrt{N_{ijk}^{\rm data}}$. For IceCube, the event count takes the form

$$N_{ij}^{\rm th} = \alpha \left[1 + \beta(0.5 + \cos(\theta_z^R)_i)\right] N_{ij}(\hat{\theta})\,, \tag{11}$$

with $N_{ij}(\hat{\theta})$ from Eq. 6. Here, we allow the event distribution to rotate around the median cosine-zenith of $\cos(\theta_z^R) = -0.5$.

For DeepCore and PINGU, and the event count takes the form

$$N_{ijk}^{\rm th} = \alpha \left[1 + \beta \cos(\theta_z^R)_i\right] N_{ijk}(\hat{\theta}) + \kappa N_{ijk}^{\mu_{atm}}\,, \tag{12}$$

with $N_{ijk}(\hat{\theta})$ from Eq. 8. $N_{ijk}^{\mu_{atm}}$ is the muon background, which is left to float freely in the DeepCore analysis. The detectors experience an uncorrelated systematic error, which comes from the muon background, i.e. events misclassified as muons from ν_μ interactions rather than from pion decay. For the DeepCore analysis, we will have to consider this background when calculating the events. For IceCube events, we scan a higher energy range where the muon background can be neglected. For the PINGU events, the IceCube detector is expected to be able to act as a veto for this background. Thus, the error introduced from the muon background is expected by the collaboration to be negligible [8]. The background at PINGU can be considered negligible to first order [16], and we thus put $\kappa = 0$ when calculating the PINGU χ^2. For DeepCore and PINGU, the median cosine-zenith is $\cos(\theta_z^R) = 0$, and we allow the event count to rotate around this point.

We treat the uncorrelated systematic uncertainties differently for each detector. For IceCube, we set $\sigma_{ij}^{\rm syst} = f\sqrt{N_{ij}^{\rm data}}$. We consider best, normal, and worst-case scenarios in IceCube using $f = 5\%$, 10%, and 15% respectively. For PINGU, we use the same form but instead use $f = 0\%$, 3%, and 5%. For DeepCore, we use the provided systematic error distribution which accounts for uncertainties in the finite MC statistics and the data-driven muon background estimate [13]. This is summarized in Table 1.

For the joint analysis, we follow the parameter goodness-of-fit prescription [18] and construct the joint χ^2 as

$$\chi^2_{\rm joint} = \sum_{\rm exp} \chi^2_{\rm exp} - \chi^2_{\rm exp,min} \tag{13}$$

Experiment	Best case	Baseline	Worst case
IceCube	5%	10%	15%
PINGU	0%	3%	5%

Table 1: Our definition of the best, baseline, and worst case scenarios considered in each experiment, modelled by $\sigma_{ijk}^{\text{syst}} = f\sqrt{N_{ijk}^{\text{data}}}$ with f from the table. We do not consider different DeepCore scenarios because her systematic error distribution is already provided in the data release [13].

with test statistic $\chi^2_{\text{joint,min}}$. The $\Delta\chi^2_{\text{joint}}$ is then $\Delta\chi^2_{\text{joint}} = \chi^2_{\text{joint}} - \chi^2_{\text{joint,min}}$.

We let each of the four NSI parameters considered assume a value, while keeping the other three fixed at zero. We consider the following ranges of values for each parameter:

$$\begin{aligned} -0.07 \leq \epsilon_{\tau\tau} \leq 0.07 \\ -0.03 \leq \epsilon_{\mu\tau} \leq 0.03 \\ -0.3 \leq \epsilon_{e\mu} \leq 0.3 \\ -0.3 \leq \epsilon_{e\tau} \leq 0.3 \end{aligned} \tag{14}$$

After the oscillation parameters Δm^2_{31}[31] and θ_{23} have been marginalized out, we plot $\Delta\chi^2$ for each of the four NSI parameters in Fig. 8. The results are shown in Fig. 9 and summarized in Tables 2 and 3. Each region is bounded by the best and worst-case scenario, as defined in Table 1, while the middle line is the baseline scenario. We again emphasize that no uncertainty scenarios are considered for DeepCore, since they already provided in the data release [13].

Comparing the PINGU and the DeepCore results in Fig. 8, we note that the best-fit for each NSI parameter for the PINGU experiment is expected to be zero. This is because the 'data' we generated during the PINGU simulations assume no NSI since they have yet to be observed in nature. This introduces a non-NSI bias in all joint analyses, which include PINGU since PINGU has stronger statistics than DeepCore and will thus pull the joint χ^2 towards $\epsilon = 0$. Moreover, we see that we can expect PINGU to be sensitive to systematic uncertainty, especially when constraining $\epsilon_{e\mu}$ and $\epsilon_{e\tau}$ from the negative side.

We compare our results to a similar analysis performed on the same DeepCore dataset in [19]. In that publication, the constraints found at 90% CL were

$$\begin{aligned} -0.055 < \epsilon_{\tau\tau} < 0.056 \\ -0.023 < \epsilon_{\mu\tau} < 0.016 \\ -0.21 < \epsilon_{e\mu} < 0.20 \\ -0.19 < \epsilon_{e\tau} < 0.20\,. \end{aligned} \tag{15}$$

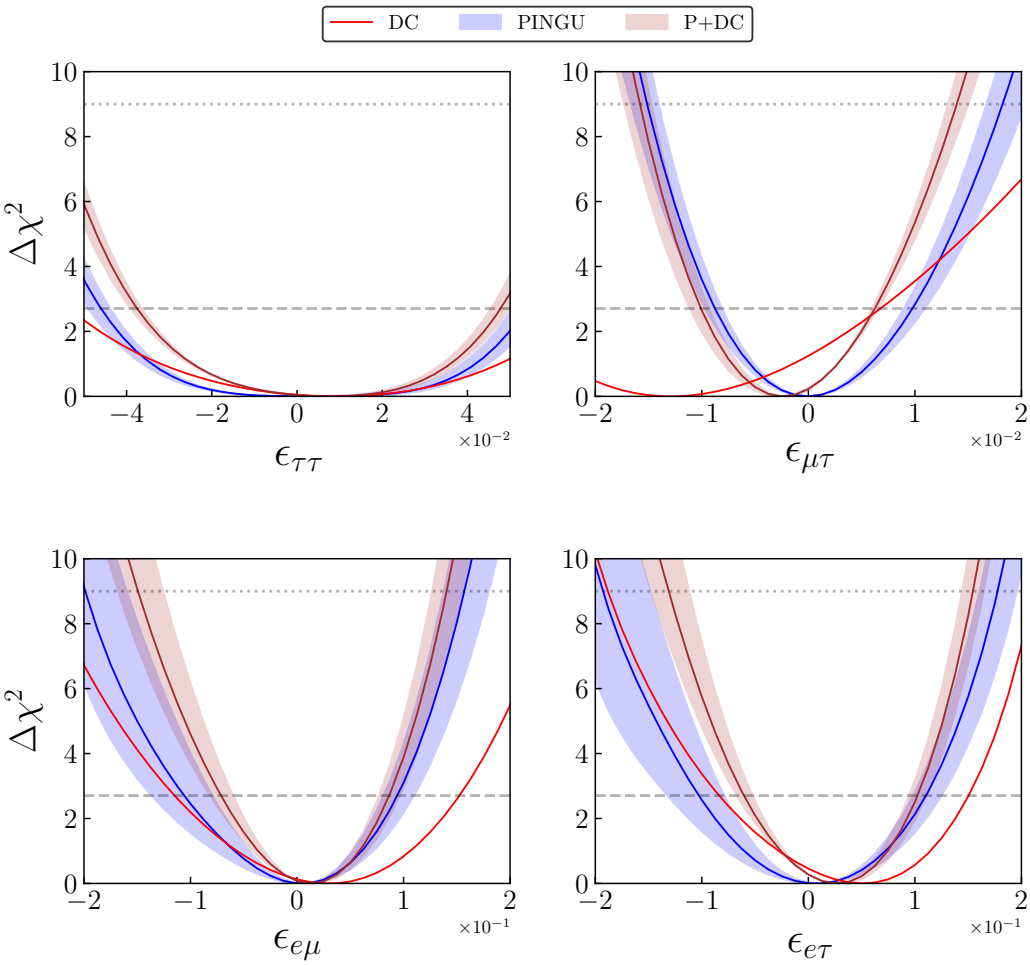

Figure 8: Confidence regions for PINGU and DeepCore scenarios listed in Table 1, with their joint $\Delta\chi^2$ in maroon. Δm^2_{31}[31] and θ_{23} and have been marginalized out, and all other NSI parameters not shown in each panel are fixed to zero. IceCube tracks only reveal $\epsilon_{\mu\tau}$, and are displayed separately in Fig. 9. Dotted lines are the 90% and 3σ CL levels.

Parameter	Best 90% CL	Best 3σ
	IceCube	
$\epsilon_{\mu\tau}$	[-0.012, 0.011]	[-0.017, 0.016]
	DeepCore	
$\epsilon_{\tau\tau}$	[-0.054, 0.067]	[-0.089, 0.10]
$\epsilon_{\mu\tau}$	[-0.029, 0.0070]	[-0.041, 0.026]
$\epsilon_{e\mu}$	[-0.12, 0.15]	[-0.23, 0.24]
$\epsilon_{e\tau}$	[-0.084, 0.15]	[-0.19, 0.21]
	IceCube + DeepCore	
$\epsilon_{\mu\tau}$	[-0.013, 0.0070]	[-0.017, 0.013]

Parameter	Baseline 90% CL	Baseline 3σ
	IceCube	
$\epsilon_{\mu\tau}$	[-0.015, 0.014]	[-0.022, 0.021]
	DeepCore	
$\epsilon_{\tau\tau}$	[-0.054, 0.067]	[-0.089, 0.10]
$\epsilon_{\mu\tau}$	[-0.029, 0.0070]	[-0.041, 0.026]
$\epsilon_{e\mu}$	[-0.12, 0.15]	[-0.23, 0.24]
$\epsilon_{e\tau}$	[-0.084, 0.15]	[-0.19, 0.21]
	IceCube + DeepCore	
$\epsilon_{\mu\tau}$	[-0.016, 0.0070]	[-0.022, 0.016]

Parameter	Worst 90% CL	Worst 3σ
	IceCube	
$\epsilon_{\mu\tau}$	[-0.018, 0.017]	[-0.025, 0.024]
	DeepCore	
$\epsilon_{\tau\tau}$	[-0.054, 0.067]	[-0.089, 0.10]
$\epsilon_{\mu\tau}$	[-0.029, 0.0070]	[-0.041, 0.026]
$\epsilon_{e\mu}$	[-0.11, 0.15]	[-0.23, 0.24]
$\epsilon_{e\tau}$	[-0.084, 0.15]	[-0.188, 0.212]
	IceCube + DeepCore	
$\epsilon_{\mu\tau}$	[-0.018, 0.0070]	[-0.024, 0.018]

Table 2: IceCube and DeepCore results from the $\Delta\chi^2$ in Fig. 9. Δm^2_{31}[31] and θ_{23} have been marginalized out, and all other NSI parameters other than the one shown for each row are set to zero. Best, baseline, and worst refer to the systematic uncertainty scenarios considered as in Table 1.

Parameter	Best 90% CL	Best 3σ
	PINGU	
$\epsilon_{\tau\tau}$	[-0.044, 0.051]	[-0.062, 0.069]
$\epsilon_{\mu\tau}$	[-0.008, 0.009]	[-0.014, 0.017]
$\epsilon_{e\mu}$	[-0.079, 0.081]	[-0.16, 0.138]
$\epsilon_{e\tau}$	[-0.079, 0.098]	[-0.148, 0.161]
	DeepCore + PINGU	
$\epsilon_{\tau\tau}$	[-0.036, 0.046]	[-0.056, 0.064]
$\epsilon_{\mu\tau}$	[-0.0090, 0.0060]	[-0.015, 0.013]
$\epsilon_{e\mu}$	[-0.060, 0.077]	[-0.13, 0.13]
$\epsilon_{e\tau}$	[-0.052, 0.095]	[-0.11, 0.14]
	IceCube + DeepCore + PINGU	
$\epsilon_{\mu\tau}$	[-0.0080, 0.0050]	[-0.012, 0.011]

Parameter	Baseline 90% CL	Baseline 3σ
	PINGU	
$\epsilon_{\tau\tau}$	[-0.046, 0.054]	[-0.065, 0.073]
$\epsilon_{\mu\tau}$	[-0.0090, 0.010]	[-0.015, 0.018]
$\epsilon_{e\mu}$	[-0.11, 0.094]	[-0.20, 0.16]
$\epsilon_{e\tau}$	[-0.10, 0.11]	[-0.19, 0.18]
	DeepCore + PINGU	
$\epsilon_{\tau\tau}$	[-0.038, 0.048]	[-0.058, 0.067]
$\epsilon_{\mu\tau}$	[-0.010, 0.0060]	[-0.016, 0.014]
$\epsilon_{e\mu}$	[-0.071, 0.086]	[-0.15, 0.14]
$\epsilon_{e\tau}$	[-0.061, 0.10]	[-0.13, 0.16]
	IceCube + DeepCore + PINGU	
$\epsilon_{\mu\tau}$	[-0.009, 0.0060]	[-0.014, 0.012]

Parameter	Worst 90% CL	Worst 3σ
	PINGU	
$\epsilon_{\tau\tau}$	[-0.049, 0.057]	[-0.07, 0.078]
$\epsilon_{\mu\tau}$	[-0.01, 0.011]	[-0.017, 0.02]
$\epsilon_{e\mu}$	[-0.137, 0.11]	[-0.228, 0.18]
$\epsilon_{e\tau}$	[-0.132, 0.125]	[-0.226, 0.196]
	DeepCore + PINGU	
$\epsilon_{\tau\tau}$	[-0.039, 0.050]	[-0.060, 0.070]
$\epsilon_{\mu\tau}$	[-0.011, 0.0070]	[-0.017, 0.015]
$\epsilon_{e\mu}$	[-0.082, 0.097]	[-0.168, 0.16]
$\epsilon_{e\tau}$	[-0.067, 0.11]	[-0.15, 0.17]
	IceCube + DeepCore + PINGU	
$\epsilon_{\mu\tau}$	[-0.010, 0.0060]	[-0.016, 0.013]

Table 3: PINGU and joint results from the $\Delta\chi^2$ in Fig. 8. Δm^2_{31}[31] and θ[23] have been marginalized out, and all other NSI parameters other than the one shown for each row are set to zero. Best, baseline, and worst refer to the systematic uncertainty scenarios considered as in Table 1.

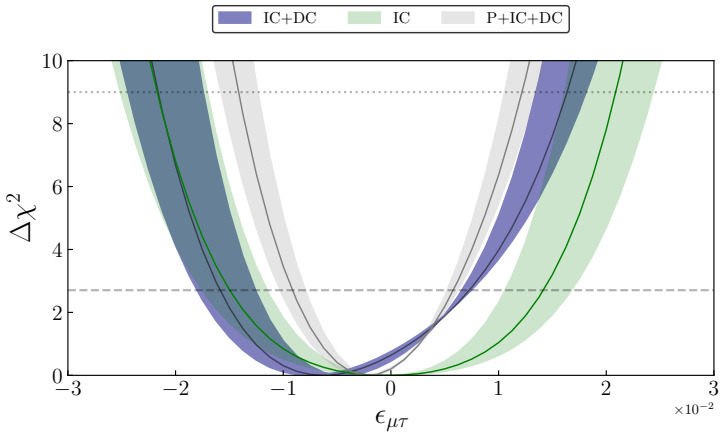

Figure 9: $\epsilon_{\mu\tau}$ $\Delta\chi^2$ regions for scenarios as defined in Table 1. Δm^2_{31}[31] and θ_{23} and have been marginalized out, and all other NSI parameters other than $\epsilon_{\mu\tau}$ are fixed to zero. Dotted lines are the 90% and 3σ CL levels. The zones contain the three uncertainty scenarios considered, and we see that the inclusion of PINGU is expected to drastically make the bound on $\epsilon_{\mu\tau}$ more stringent.

	Best fit		
Parameter	Δm^2_{31}[31]	θ_{23}	ϵ
	DeepCore		
$\epsilon_{\tau\tau}$	2.435	47.84	0.0125
$\epsilon_{\mu\tau}$	2.435	43.97	-0.005
$\epsilon_{e\mu}$	2.435	43.97	0
$\epsilon_{e\tau}$	2.435	43.97	0.05
	IceCube		
$\epsilon_{\mu\tau}$	2.435	51.70	0
	IceCube + DeepCore		
$\epsilon_{\mu\tau}$	2.517	43.97	-0.01

Table 4: Best fit points for Δm^2_{31}[31] and θ_{23} are given in units of 10^{-3}eV^2 and degrees, respectively.

Comparing 15 to our results from Table 2 at 90% CL, namely

$$\begin{aligned} -0.054 &< \epsilon_{\tau\tau} < 0.067 \\ -0.029 &< \epsilon_{\mu\tau} < 0.0070 \\ -0.12 &< \epsilon_{e\mu} < 0.15 \\ -0.084 &< \epsilon_{e\tau} < 0.15\,, \end{aligned} \tag{16}$$

we see that our results for $\epsilon_{e\mu}$, $\epsilon_{e\tau}$ are more stringent, while the results for $\epsilon_{\mu\tau}$ and $\epsilon_{\tau\tau}$ are similar but more lenient. It is worth noting that the results from [19] are have been obtained by including more systematic uncertainties, such as the spectral index, hadron production, and baryon resonance. However, the overall flux normalization in [19] is 20%, while we opted for a slightly higher figure of 25%, which could compensate for the exclusion of the statistical uncertainties mentioned.

Using the baseline case of 3% systematic uncertainty at 90% CL, we find from Table 3, that our predictions for the proposed PINGU detector are

$$\begin{aligned} -0.049 &< \epsilon_{\tau\tau} < 0.057 \\ -0.010 &< \epsilon_{\mu\tau} < 0.011 \\ -0.137 &< \epsilon_{e\mu} < 0.11 \\ -0.132 &< \epsilon_{e\tau} < 0.125\,, \end{aligned} \tag{17}$$

which displays an improvement over the DeepCore results in Eq. 16, except for $\epsilon_{e\tau}$ which is worse.

Finally, the joint results for $\epsilon_{\mu\tau}$ using IceCube and DeepCore from 3 at 90% CL are

$$-0.016 < \epsilon_{\mu\tau} < 0.0070\,, \tag{18}$$

and when combining IceCube, DeepCore, and PINGU, the 90% CL constraint on $\epsilon_{\mu\tau}$ in our baseline scenario is predicted to be

$$-0.010 < \epsilon_{\mu\tau} < 0.0060\,, \tag{19}$$

which is more stringent for $\epsilon_{\mu\tau} > 0$ than the result in [1].

We plot the event pull $(N_{NSI} - N_{SI})/\sqrt{N_{SI}}$ where $N_{(N)SI}$ are the numbers of expected events assuming (non-)standard interactions in Fig. 10. This gives the normalized difference in the number of expected events at the detector and illustrates the expected sensitivity of DeepCore for the NSI parameters.

Now we will compare the probability plots with the final event counts in DeepCore. It is not enough to only study the effect at probability level, since that is in true quantities. Since the detector data comes in reconstructed quantities, it might be the case that a feature at probability level gets averaged out in the reconstruction, and not showing up at all in the data. In general, features showing at probability level are can be averaged out at reconstruction if they occur in the rapidly oscillating part of single-digit GeV energies.

The top right panel shows a surplus of DeepCore track events at 20 GeV to 30 GeV for through-going neutrinos when we turn on $\epsilon_{\tau\tau}$. This is what we expected from the bottom right panel in Fig. 1, where we saw that we had an increase in $\bar{\nu}_\mu$ survival probability at 20 GeV to 40 GeV.

The third right panel shows the expected event pull for $\epsilon_{e\mu}$. Comparing with the probabilities in Fig. 2, we see that the surplus of the $\bar{\nu}_\mu$ survival in the 20 GeV to 30 GeV and the deficit above 40 GeV is intact, while the 10 GeV ν_μ deficit is completely averaged out.

There is no reason for us to assume that only one NSI parameter exists in Nature, unless we impose a symmetry on the gauge group which generates NSI. So ideally, we would simulate a grid where all NSI parameters are allowed to vary, but this is not feasible. Thus, we take we set $\epsilon_{\tau\tau} = 0$ and let $\epsilon_{\mu\tau}, \epsilon_{e\mu}, \epsilon_{e\tau}$ vary, along with Δm^2_{31}[31] and θ_{23}. We let $\epsilon_{\tau\tau} = 0$ because we saw that it did not influence the other parameters. We then marginalize out the standard oscillation parameters and one of the NSI parameters and plot the remaining two in Fig. 11. We see that the pairs $\epsilon_{e\mu} - \epsilon_{\mu\tau}$ and $\epsilon_{e\tau} - \epsilon_{\mu\tau}$ are symmetrical. Hence, we can see that no relationship exists between them. With $\epsilon_{e\tau} - \epsilon_{e\mu}$, however, the contours are assuming a different shape. The contour allows positive values of $\epsilon_{e\tau}$ and $\epsilon_{e\mu}$ to a greater degree than mixed or negative values. Thus, we can draw the conclusion that, given $\epsilon_{\tau\tau} = 0$, PINGU might expect to observe that $\epsilon_{e\mu}$ and $\epsilon_{\mu\tau}$ are anti-correlated while we expect no significant correlation to be be seen between the pairs $\epsilon_{\mu\tau} - \epsilon_{e\mu}$, and $\epsilon_{\mu\tau} - \epsilon_{e\tau}$. This is consistent with our observation of the effect of these parameters on $P_{\mu e}$ in Fig. 5, from which we saw that $\epsilon_{e\mu}$ and $\epsilon_{e\tau}$ strongly affect $P_{\mu e}$ for single-digit GeV energies.

3.2 Conclusion

We introduced Non-Standard Interactions (NSI) in Sec. 1 as a possible example of new physics beyond the Standard Model. We then studied the effects of NSI on the neutrino oscillation probabilities and saw that NSI effects other than those stemming from $\epsilon_{\mu\tau}$ are not apparent in the TeV region. Moreover, we saw in $P_{\mu e}$ that we could expect a correlation between $\epsilon_{e\mu}$ and $\epsilon_{e\tau}$ in the single-digit GeV range. We also saw that $\epsilon_{\mu\tau}$ effects were visible on probability level in both the GeV and TeV regions.

We simulated the 86 string IceCube detector with track events, explained in Sec. 2.1. In Sec. 3.1, we studied the NSI parameter $\epsilon_{\mu\tau}$ and its effect events captured by IceCube. Using a χ^2 test, we found that the bound from IceCube on $\epsilon_{\mu\tau}$ at 90 % confidence level was

$$-0.015 < \epsilon_{\mu\tau} < 0.014 \quad (90\% \text{ CL}) \tag{20}$$

for our 'baseline' case of 15% uncorrelated systematic uncertainty.

In Sec. 2.2, we moved on and explained our method of simulating a second detector, DeepCore. Armed with simulations possible for this detector, we then continued to explore the possibility of NSI, this time including both track and cascade events and a lower energy region. Using the χ^2 test defined in Eq. 10 and

after marginalizing Δm^2_{31}[31] and θ_{23} out, we found the following constraints on the NSI parameters at 90% confidence level:

$$\begin{aligned} -0.054 &< \epsilon_{\tau\tau} < 0.067 \\ -0.029 &< \epsilon_{\mu\tau} < 0.0070 \\ -0.12 &< \epsilon_{e\mu} < 0.15 \\ -0.084 &< \epsilon_{e\tau} < 0.15 \quad \text{(all at 90\% CL)}\,. \end{aligned} \tag{21}$$

We compared these constraints to literature and found that the bounds for $\epsilon_{e\mu}$ and $\epsilon_{e\tau}$ were more stringent than those obtained in [19]. Then, we did a joint χ^2 test using simulated events from both IceCube and DeepCore. At 90% confidence level, the bound of $\epsilon_{\mu\tau}$ improved to

$$-0.016 < \epsilon_{\mu\tau} < 0.0070 \quad \text{(90\% CL)}\,. \tag{22}$$

In Sec. 2.3 we described our method of simulating a proposed upgrade to the IceCube array: PINGU. Since PINGU is not yet live, we produced data for it assuming a standard 3 neutrino hypothesis with parameters from [17]. After a χ^2 analysis, we obtained the following constrains on the NSI parameters at 90% confidence level:

$$\begin{aligned} -0.049 &< \epsilon_{\tau\tau} < 0.057 \\ -0.010 &< \epsilon_{\mu\tau} < 0.011 \\ -0.137 &< \epsilon_{e\mu} < 0.11 \\ -0.132 &< \epsilon_{e\tau} < 0.125 \quad \text{(all at 90\% CL)}\,. \end{aligned} \tag{23}$$

After that, we did a joint χ^2 analysis combining IceCube, DeepCore and simulated PINGU events to further constrict $\epsilon_{\mu\tau}$. The bound at 90% confidence level obtained was

$$-0.010 < \epsilon_{\mu\tau} < 0.0060\,. \quad \text{(90\% CL)} \tag{24}$$

We were then able to draw the conclusion that we expect PINGU to successfully be able to observe the impact of NSI. Moreover, a joint analysis between PINGU and at least one of the other detectors under the IceCube collaboration will be able to constrain the parameters even further. We saw that can expect PINGU to be more sensitive to NSI effects than DeepCore. We were also able to see that when constraining $\epsilon_{e\mu}$ and $\epsilon_{e\tau}$ from the negative side, we can expect the result to be highly dependent on the systematic uncertainty of PINGU.

Finally, we simulated the event count in PINGU, allowing $\epsilon_{\mu\tau}$, $\epsilon_{e\mu}$, and $\epsilon_{e\tau}$ to vary, but setting $\epsilon_{\tau\tau} = 0$. After and marginalizing out Δm^2_{31}[31], θ_{23}, and $\epsilon_{\mu\tau}$, we saw that the effect of $\epsilon_{e\mu}$ and $\epsilon_{e\tau}$ on $P_{\mu e}$ had indeed propagated through to the event count, manifesting as an anti-correlation between the $\epsilon_{e\mu}$ and $\epsilon_{e\tau}$ at both 90% and 3σ confidence levels. No other pair of NSI parameters were observed to have a significant correlation.

References

[1] The IceCube Collaboration, Search for nonstandard neutrino interactions with IceCube DeepCore 97 (7) 072009. doi:10.1103/PhysRevD.97.072009.

[2] A. M. Dziewonski and D. L. Anderson, Preliminary reference Earth model 25 (4) 297–356. doi:10.1016/0031-9201(81)90046-7.

[3] A. Esmaili and A. Y. Smirnov, Probing Non-Standard Interaction of Neutrinos with IceCube and DeepCore 2013 (6) 26. arXiv:1304.1042, doi:10.1007/JHEP06(2013)026.

[4] S. Choubey and T. Ohlsson, Bounds on Non-Standard Neutrino Interactions Using PINGU 739 357–364. doi:10.1016/j.physletb.2014.11.010.

[5] T. Ohlsson et al., Effects of nonstandard neutrino interactions at PINGU 88 (1) 013001. doi:10.1103/PhysRevD.88.013001.

[6] M. Honda et al., Calculation of atmospheric neutrino flux using the interaction model calibrated with atmospheric muon data.doi:10.1103/PhysRevD.75.043006.

[7] The IceCube Collaboration, All-flavor constraints on nonstandard neutrino interactions and generalized matter potential with three years of IceCube DeepCore data. arXiv:2106.07755.

[8] The IceCube Gen2 Collaboration, Letter of Intent: The Precision IceCube Next Generation Upgrade (PINGU). arXiv:1401.2046.

[9] The IceCube Collaboration et al., Searching for eV-scale sterile neutrinos with eight years of atmospheric neutrinos at the IceCube Neutrino Telescope 102 (5) 052009. doi:10.1103/PhysRevD.102.052009.

[10] The IceCube Collaboration, All-sky point-source IceCube data: Years 2010-2012. doi:10.21234/B4F04V.

[11] C. Weaver, Evidence for Astrophysical Muon Neutrinos from the Northern Sky.

[12] The IceCube Collaboration, Search for sterile neutrinos with one year of IceCube data.
URL https://icecube.wisc.edu/data-releases/2016/06/search-for-sterile-neutrinos-with-one-year-of-icecube-data/

[13] The IceCube Collaboration, Three-year high-statistics neutrino oscillation samples. doi:10.21234/ac23-ra43.

[14] The IceCube Collaboration, Measurement of Atmospheric Neutrino Oscillations at 6–56 GeV with IceCube DeepCore 120 (7) 071801. doi:10.1103/PhysRevLett.120.071801.

[15] The IceCube Collaboration, Measurement of atmospheric tau neutrino appearance with IceCube DeepCore 99 (3) 032007. doi:10.1103/PhysRevD.99.032007.

[16] The IceCube Collaboration, IceCube Upgrade Neutrino Monte Carlo Simulation. doi:10.21234/qfz1-yh02.

[17] I. Esteban et al., The fate of hints: Updated global analysis of three-flavor neutrino oscillations 2020 (9) 178. doi:10.1007/JHEP09(2020)178.

[18] M. Maltoni and T. Schwetz, Testing the statistical compatibility of independent data sets 68 (3) 033020. arXiv:hep-ph/0304176, doi:10.1103/PhysRevD.68.033020.

[19] S. Demidov, Bounds on non-standard interactions of neutrinos from IceCube DeepCore data 2020 (3) 105. doi:10.1007/JHEP03(2020)105.

DeepCore (2017)

- ✓ Honda atmospheric fluxes
- × Only look at tracks and $\epsilon_{\mu\tau}$
- × DC Monte Carlo from an older dataset
- × 8 E bins from $6.3\,\mathrm{eV}^2$ to $56\,\mathrm{eV}^2$
- × 8 z bins from -1 to 0
- × Use "Overall" and "relative ν_e to ν_μ" normalization
- × Prior on spectral index
- × No zenith angle normalization
- ✓ No priors on $\Delta m^2_{31}, \theta_{23}, \theta_{13}$

Demidov (2020) DC analysis

- ✓ Honda atmospheric fluxes
- ✓ Looks at tracks + cascades for $\epsilon_{\mu\tau}$ and $\epsilon_{\tau\tau}$
- ✓ Data and Monte Carlo from DC 2018
- ✓ 8 E bins from $5.6\,\mathrm{eV}^2$ to $56\,\mathrm{eV}^2$
- ✓ 8 z bins from -1 to 1
- × Use "Overall" and "relative ν_e to ν_μ" normalization
- × Prior on spectral index
- × No zenith angle normalization
- ✓ No priors on $\Delta m^2_{31}, \theta_{23}$
- ✓ Fixes $\Delta m^2_{21}, \theta_{12}, \theta_{13}$
- × Uncertainty on hadron production in atmosphere
- × Uncertainty on neutrino nucleon cross section

This DC+PINGU analysis

- ✓ Honda atmospheric flu
- ✓ Tracks and cascades fo vors
- ✓ Reco → true mappi Monte Carlo migration
- ✓ 8 E bins from $5.6\,\mathrm{eV}^2$ t
- ✓ 8 zenith angle bins fro 1
- ✓ Flux normalization tainty of 25%
- ✓ Zenith angle uncertain
- ✓ No priors on oscillat rameters
- ✓ Marginalize Δm^2_{31} a All other oscillation ters are fixed.

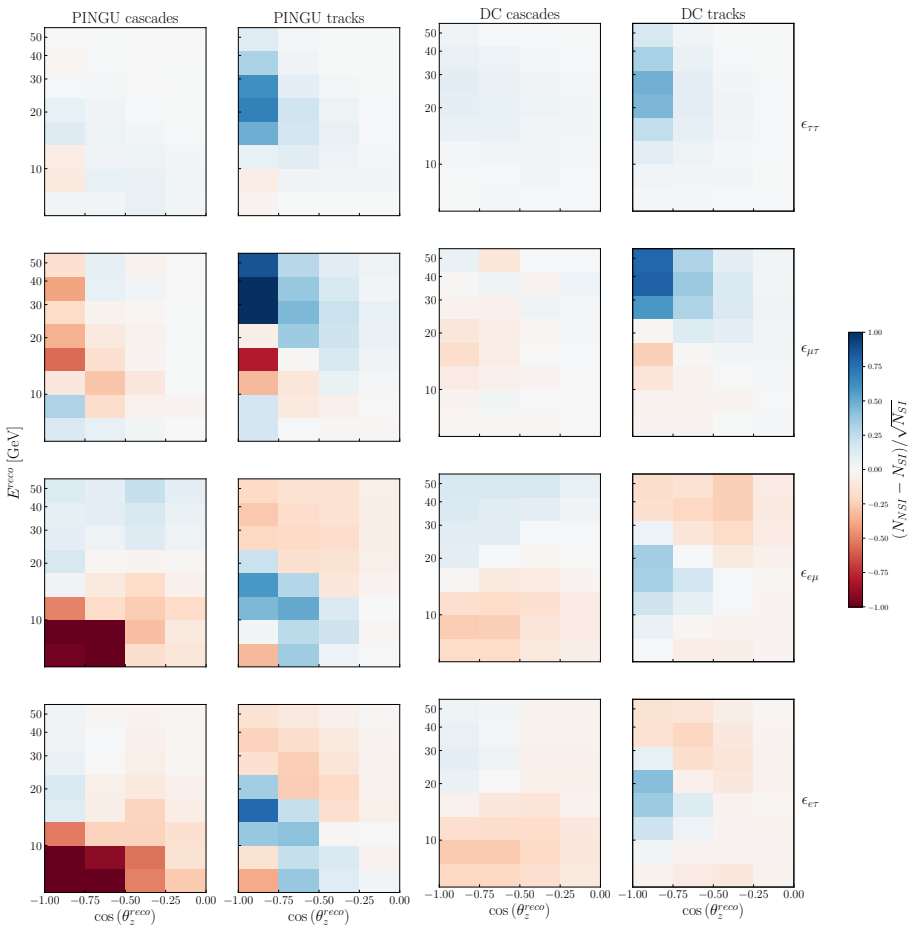

(a) PINGU (b) DeepCore

Figure 10: Expected pulls of the form $(N_{NSI} - N_{SI})/\sqrt{N_{SI}}$ for PINGU and DeepCore after 3 years of data. Each row has only one NSI non-zero parameter, with the first row having $\epsilon_{\tau\tau} = -0.07$, second $\epsilon_{\mu\tau} = -0.03$, third $\epsilon_{e\mu} = -0.3$, and fourth $\epsilon_{e\tau} = -0.3$. We clearly see the increased statistics of the PINGU detector, especially in cascade events. The low values of $\epsilon_{\tau\tau}$ and $\epsilon_{\mu\tau}$ produce a weak pull in DeepCore, while PINGU can be expected to observe multiple regions of strong pulls for $\epsilon_{\mu\tau}$, $\epsilon_{e\mu}$, and $\epsilon_{e\tau}$.

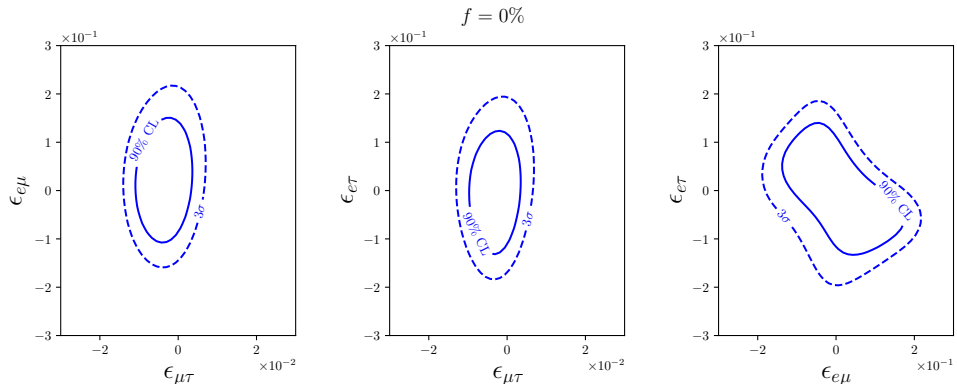

Figure 11: Allowed regions for some of the NSI parameters after three years of PINGU data, assuming no uncorrelated systematic error. All plots are made with $\epsilon_{\tau\tau} = 0$. The two standard oscillation parameters Δm^2_{31}[31] and θ_{23} along with the one NSI parameter not shown have been marginalized out. We observe an anti-correlation between $\epsilon_{e\mu}$ and $\epsilon_{e\tau}$, consistent with our observation of the effect of these parameters on $P_{\mu e}$ in Fig. 5. The values of the standard oscillation parameters are taken from NuFit [17].